Vol 17 No 11, November 2008
1674-1056/2008/17(11)/4292-08

Chinese Physics B

© 2008 Chin. Phys. Soc.
and IOP Publishing Ltd

Theoretical study of electromechanical property in a p-type silicon nanoplate for mechanical sensors*

Zhang Jia-Hong(张加宏), Huang Qing-An(黄庆安)†,
Yu Hong(于 虹), and Lei Shuang-Ying(雷双瑛)

Key Laboratory of MEMS of Ministry of Education, Southeast University, Nanjing 210096, *China*

(Received 28 April 2008; revised manuscript received 29 May 2008)

Electromechanical property of a p-type single-crystal silicon nanoplate is modelled by a microscopic approach where the hole quantization effect and the spin–orbit coupling effect are taken into account. The visible anisotropic subband structures are calculated by solving self-consistently the stress-dependent 6×6 $\boldsymbol{k}\cdot\boldsymbol{p}$ Schrödinger equation with the Poisson equation. The strong mixing among heavy, light, and split-off holes is quantitatively assessed. The influences of the thickness and the temperature on the piezoresistive coefficient are quantitatively investigated by using the hole concentrations and the effective masses from the complex dispersion structure of the valence band with and without stresses. Our results show that the stress determines the extent to which the band is mixed. The hole quantization effect increases as the thickness decreases, and therefore the valence band is strongly reshaped, resulting in the size-dependent piezoresistivity of the silicon nanoplate. The piezoresistive coefficient increases almost 4 times as the thickness reduces from the bulk to 3 nm, exhibiting a promising application in mechanical sensors.

Keywords: silicon nanoplate, piezoresistive, band structure, band mixing
PACC: 7220F, 7320D, 7320A

1. Introduction

Since the discovery of the piezoresistive effect in silicon,[1] there have been conducted a lot of theoretical and experimental studies on the piezoresistive effect.[2−10] With the advance of the nanotechnology in recent years, there is an increasing interest in the piezoresistive effect in nanoplates[11−14] or nanowires.[15,16] The purpose of recent work tends to use nanoscale silicon as an active material for mechanical sensors, especially ultrasensitive sensors for ultrafine resolution applications. For instance, the high-sensitivity piezoresistive cantilevers (nanoplates) under 100 nm thick, which are used for atomic force microscopy, have been constructed.[17] They constitute a promising approach as sensors for detecting chemical and biological interactions. Recently, the piezoresistance in p-type single-crystal silicon nanowires has been investigated experimentally and found that its piezoresistive coefficient could increase up to 50% compared with the classical value,[18] which has created a new degree of freedom for improving the performance of mechanical sensors without considerably increasing the cost and complexity of fabrication. More recently, a theoretical model[19] was introduced to the study of the piezoresistive properties of the silicon nanoplate. They applied the analytical solution to a four-band $\boldsymbol{k}\cdot\boldsymbol{p}$ Hamiltonian[20] for eigenvalues and eigenfunctions. However, in this way, the complete band structure of the silicon nanoplate was not given, and the warping of the energy surface in the valence band and the spin–orbit coupling effect on the valence-band structure were neglected. This leads to the overestimated enhancement of the piezoresistive coefficient obtained by considering only the heavy and light hole couplings.

In this paper we present a detailed theoretical analysis of subband structure and electromechanical property of a p-type single-crystal silicon nanoplate by using a full six-band $\boldsymbol{k}\cdot\boldsymbol{p}$ model where the hole quantization effect, the effect of band mixing, the spin orbit interactions as well as the mechanical stress are taken in to account quantitatively. It shows that the silicon nanoplate has qualitatively enhanced the piezoresistive property, which is due to the interaction of the piezoresistive effect with the hole quantization effect.

*Project supported by the National Basic Research Program of China (Grant No 2006CB300404), and the National High-Technology Research and Development Program of China (Grant No 2007AA04Z301).
†Corresponding author. E-mail: hqa@seu.edu.cn

2. Theory model

In our theoretical approach, a p-type single-crystal silicon nanoplate is considered, whose orientation is taken to be along [110], and the wafer is (001) surface-oriented with a doping concentration of $1 \times 10^{17}\mathrm{cm}^{-3}$. To describe the valence-band structure and compute the hole concentration, the following wavefunction equation has to be solved:

$$[\widehat{\boldsymbol{H}}_h(k_x, k_y, k_z = -\mathrm{i}\partial/\partial z) + \boldsymbol{I}\boldsymbol{V}(z)] \cdot \boldsymbol{\psi}_{n,k_x,k_y}(z) = \boldsymbol{E}_n(k_x, k_y)\boldsymbol{\psi}_{n,k_x,k_y}(z), \quad (1)$$

where $\boldsymbol{I}$ is the 6×6 identity matrix, and $\boldsymbol{V}(z)$ is the electrostatic potential for holes along the z direction. In all cases computed, it is assumed that holes are almost completely confined to the nanoplate (the barrier potential is set to be 4.6 eV such that the wave functions decay strongly outside the silicon nanoplate surface.). $\boldsymbol{\psi}_{n,k_x,k_y}(z)$ is a six-vector subject to the Dirichlet boundary conditions $\boldsymbol{\psi}_{n,k_x,k_y}(0) = 0$ and $\boldsymbol{\psi}_{n,k_x,k_y}(\boldsymbol{L}_z) = 0$ ($\boldsymbol{L}_z$ is the effective thickness of the silicon nanoplate), and the full 6×6 Hamiltonian in the envelope-function space, including strain and spin-off effects, is given by[21]

$$\boldsymbol{H}_{\mathrm{h}} = -\begin{bmatrix} \boldsymbol{P}+\boldsymbol{Q} & -\boldsymbol{S} & \boldsymbol{R} & 0 & -\frac{1}{\sqrt{2}}\boldsymbol{S} & \sqrt{2}\boldsymbol{R} \\ -\boldsymbol{S}^{+} & \boldsymbol{P}-\boldsymbol{Q} & 0 & \boldsymbol{R} & -\sqrt{2}\boldsymbol{Q} & \sqrt{\frac{3}{2}}\boldsymbol{S} \\ \boldsymbol{R}^{+} & 0 & \boldsymbol{P}-\boldsymbol{Q} & \boldsymbol{S} & \sqrt{\frac{3}{2}}\boldsymbol{S}^{+} & \sqrt{2}\boldsymbol{Q} \\ 0 & \boldsymbol{R}^{+} & \boldsymbol{S}^{+} & \boldsymbol{P}+\boldsymbol{Q} & -\sqrt{2}\boldsymbol{R}^{+} & -\frac{1}{\sqrt{2}}\boldsymbol{S}^{+} \\ -\frac{1}{\sqrt{2}}\boldsymbol{S}^{+} & -\sqrt{2}\boldsymbol{Q} & \sqrt{\frac{3}{2}}\boldsymbol{S} & -\sqrt{2}\boldsymbol{R} & \boldsymbol{P}+\boldsymbol{\Delta} & 0 \\ \sqrt{2}\boldsymbol{R}^{+} & \sqrt{\frac{3}{2}}\boldsymbol{S}^{+} & \sqrt{2}\boldsymbol{Q} & -\frac{1}{\sqrt{2}}\boldsymbol{S} & 0 & \boldsymbol{P}+\boldsymbol{\Delta} \end{bmatrix}, \quad (2)$$

where

$$\begin{aligned} &\boldsymbol{P} = \boldsymbol{P}\boldsymbol{\kappa} + \boldsymbol{P}\boldsymbol{\varepsilon}, \quad M\boldsymbol{Q} = \boldsymbol{Q}\boldsymbol{\kappa} + \boldsymbol{Q}\boldsymbol{\varepsilon}, \quad \boldsymbol{R} = \boldsymbol{R}\boldsymbol{\kappa} + \boldsymbol{R}\boldsymbol{\varepsilon}, \quad \boldsymbol{S} = \boldsymbol{S}\boldsymbol{\kappa} + \boldsymbol{S}\boldsymbol{\varepsilon}, \\ &\boldsymbol{P}\boldsymbol{\kappa} = \left(\frac{\hbar^2}{2m_0}\right)\gamma_1\left(k_x^2 + k_y^2 - \frac{\partial^2}{\partial z^2}\right) - \boldsymbol{E}_v, \quad \boldsymbol{P}\boldsymbol{\varepsilon} = -a\left(\varepsilon_{xx} + \varepsilon_{yy} + \varepsilon_{zz}\right), \\ &\boldsymbol{Q}\boldsymbol{\kappa} = \left(\frac{\hbar^2}{2m_0}\right)\gamma_2\left(k_x^2 + k_y^2 + 2\frac{\partial^2}{\partial z^2}\right), \quad \boldsymbol{Q}\boldsymbol{\varepsilon} = -\frac{b}{2}\left(\varepsilon_{xx}\varepsilon_{yy} - 2\varepsilon_{zz}\right), \\ &\boldsymbol{R}\boldsymbol{\kappa} = \left(\frac{\hbar^2}{2m_0}\right)\sqrt{3}\left[-\gamma_2\left(k_x^2 - k_y^2\right) + 2\mathrm{i}\gamma_3 k_x k_y\right], \quad \boldsymbol{R}\boldsymbol{\varepsilon} = \frac{\sqrt{3b}}{2}\left(\varepsilon_{xx}\varepsilon_{yy}\right) - \mathrm{id}\varepsilon_{zz}, \\ &\boldsymbol{S}\boldsymbol{\kappa} = -\left(\frac{\hbar^2}{2m_0}\right)2\sqrt{3}\gamma_3\left(k_y + \mathrm{i}k_x\right)\frac{\partial}{\partial z}, \quad \boldsymbol{S}\boldsymbol{\varepsilon} = -d\left(\varepsilon_{zx} - \mathrm{i}\varepsilon_{yz}\right), \end{aligned} \quad (3)$$

where m_0 is the free electron mass, γ_i is the Luttinger parameters, a, b, and d are the Bir–Pikus deformation potentials, which can be directly measured experimentally, and their values are well-known for silicon,[22] Δ is the spin–orbit split-off energy, ε_{ij} is the symmetric strain tensor, $\boldsymbol{E}_v$ is the valence band edge energy. For the silicon nanoplate, as there is no translation invariance along the z direction, replacing the wave vector k_z with its differential operator notation as $k_z = -\mathrm{i}\partial/\partial z$, and using the three-point finite-difference method, Eq.(1) can be recast into an eigenvalue equation for the in-plane eigenenergies at different values of the in-plane wave-vector, $\boldsymbol{K}_{//}(k_x, k_y)$. The solution to the eigenvalue problem involves the diagonalization of a $6N_z \times 6N_z$ tridiagonal block matrix

$$\begin{bmatrix} \cdot & \cdot & \cdot & \cdot & \cdot & \cdot & \cdot \\ \cdot & \widehat{\boldsymbol{D}}_{\rm bot} & \widehat{\boldsymbol{D}}_{l-1} & \widehat{\boldsymbol{D}}_{\rm top} & 0 & 0 & \cdot \\ \cdot & 0 & \widehat{\boldsymbol{D}}_{\rm bot} & \widehat{\boldsymbol{D}}_{l} & \widehat{\boldsymbol{D}}_{\rm top} & 0 & \cdot \\ \cdot & 0 & 0 & \widehat{\boldsymbol{D}}_{\rm bot} & \widehat{\boldsymbol{D}}_{l+1} & \widehat{\boldsymbol{D}}_{\rm top} & \cdot \\ \cdot & \cdot & \cdot & \cdot & \cdot & \cdot & \cdot \end{bmatrix} \begin{bmatrix} \cdot \\ \boldsymbol{\psi}_{l-1} \\ \boldsymbol{\psi}_{l} \\ \boldsymbol{\psi}_{l+1} \\ \cdot \end{bmatrix} = \boldsymbol{E}(\boldsymbol{K}_{//}) \begin{bmatrix} \cdot \\ \boldsymbol{\psi}_{l-1} \\ \boldsymbol{\psi}_{l} \\ \boldsymbol{\psi}_{l+1} \\ \cdot \end{bmatrix}, \tag{4}$$

where N_z is the number of mesh points along the quantization direction in the real space, $\widehat{\boldsymbol{D}}_l$, $\widehat{\boldsymbol{D}}_{\rm top}$, and $\widehat{\boldsymbol{D}}_{\rm bot}$ $\widehat{\boldsymbol{D}}^{+}_{\rm top}$ are 6×6 block-diagonal difference operators, functions of $\boldsymbol{K}_{//}\,(k_x, k_y)$.

If an initial potential V_0 is assumed, Eq.(4) is first solved, $\boldsymbol{E}_n(k_x, k_y)$ and $\boldsymbol{\psi}_{n,k_x,k_y}(z)$ are then obtained. Thus the density of carriers, $p(z)$, can be calculated by

$$p(z) = \sum_{n=\text{subbands}} \int \frac{\mathrm{d}^2 \boldsymbol{K}_{//}}{4\pi^2} \times f[\boldsymbol{E}_n(k_x, k_y)] \times \left|\varphi_{n,k_x,k_y}(z)\right|^2, \tag{5}$$

where

$$f[\boldsymbol{E}_n(k_x, k_y)] = \{1+\exp[(\boldsymbol{E}_{\rm f} - \boldsymbol{E}_n(k_x, k_y))/(k_{\rm B}T)]\}^{-1}$$

is the Fermi–Dirac function for holes, $k_{\rm B}$ is the Boltzmann constant, and $\left|\varphi_{n,k_x,k_y}(z)\right|^2 \cong \left|\boldsymbol{\psi}_{n,k_x,k_y}(z)\right|^2$. At a given temperature T, based on charge conservation law,[23] the numerical evaluation of the Fermi level, $E_{\rm f}$, is performed by using Newton's methods. Once $p(z)$ is obtained, we can obtain the electrostatic potential $\boldsymbol{V}(z)$ by further solving the Poisson equation. The Poisson equation is given by

$$-\frac{\partial^2 \boldsymbol{V}(z)}{\partial z^2} = \frac{e}{\varepsilon}[p(z) - N_{\rm A}(z) - n(z)], \tag{6}$$

where $p(z)$, $n(z)$, and $N_A(z)$ are the hole density, the electron density, and the ionized acceptor density, respectively. With the new $\boldsymbol{V}(z)$, and using Eqs.(4) and (5), we calculate $p(z)$ once again. It keeps continuing iteratively until convergence is achieved.

3. Results

3.1. Valence-band structures

As expected, due to the quantum size-effect, the valence band of a strained-silicon nanoplate obtained by using the full six-band $\boldsymbol{k}\cdot\boldsymbol{p}$ model is reshaped. The influence of the quantum confinement of holes on the band structure not only splits the heavy hole (HH), light hole (LH) and split-off hole (SO) bands into subbands, but also results in the separation of HH and LH subbands under no stress. This leads to strong variations in population distribution of holes and in effective mass, implying different electromechanical properties from those of the bulk counterpart. The valence-band structures for the lowest quantized subbands demonstrate obvious anisotropy as illustrated in Fig.1. It is apparent from the figures that the warped band structure depends on both $\boldsymbol{K}_{//}$ and stress. The greater the value of $\boldsymbol{K}_{//}$is, the more noticeable the warping will be. Therefore, it is a very crude approximation in hole study to consider the bands to be parabolic, and so the complex dispersion characteristics should be considered. The appropriate modelling of the dispersion near the Γ point ($\boldsymbol{K}_{//}$=0) is important as it provides the highest hole occupation. Figure 1(a) corresponds to HH-like subband near the Γ point, while Figs.1(b) and 1(c) have a mixture of LH-like and SO-like characteristics. Note that the Γ point in Fig.1(c) is characterized by reversed camel back structures with negative hole effective mass, which means that some states in hole subbands behave like conduction-band electrons near the Γ point. The electron-like effective mass has to be considered, and especially the contribution of SO band is significantly large in the simulation of electromechanical property.

It is useful to illustrate anisotropic isoenergetic lines of subbands in the cases with and without stresses, since the origin of piezoresistive effect can be qualitatively explained by using the shape change of isoenergetic lines at the presence of deformation. For example, the isoenergetic lines of the n=1 subband with and without stresses are shown in Fig.1(d). Under the zero stress condition, the heavy holes are equally located in the four wings I1, I2, I3, and I4 enclosed by the isoenergetic lines. However, it is clear that I2 and I4 have a small curvature along the [110]

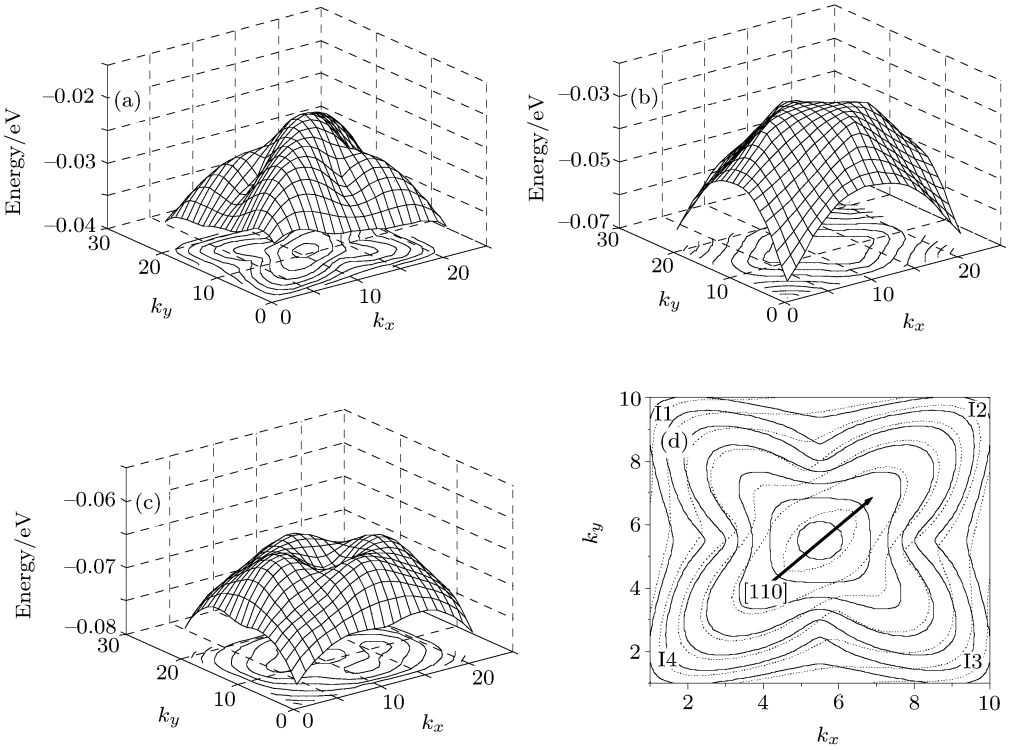


Fig.1. Warped band structure in the $k_x - k_y$ plane with 100MPa mechanical tensile stress along the [110] direction. Panels (a), (b), and (c) correspond respectively to the first three subbands. The isoenergetic lines related to each subband have also been plotted. Panel (d) is isoenergetic lines of the n=1 subband without stress (solid lines) and with 100MPa stress (dotted lines) for a silicon nanoplate.

direction than I1 and I3, so carriers sitting on I2 and I4 will have a heavier effective mass than those sitting on I1 and I3. On the application of 100MPa [110] tensile stress, an increase in effective mass along the [110] direction due to the strain is visible. In addition, stronger anisotropic isoenergetic lines are produced by the stress. The wings can be moved up and down in energy, and Fig.1(d) shows the lowering of the I2 and I4 wings and the rising of the I1 and I3 wings, resulting in a hole repopulation from the low transport effective mass regions I1 and I3 to the high transport effective mass regions I2 and I4. Therefore , the origin of the piezoresistive effect of a p-type single-crystal silicon nanoplate is still based on the change in hole concentration and the change in transport effective mass.

In order to assess the band mixing effect quantitatively and study further the spin–orbit coupling effect, the nature of the subbands has been calculated as[24]

$$
\begin{aligned}
P_{\mathrm{HH},n,k_x,k_y} &= \frac{100\int\left\{\left|\boldsymbol{\psi}_{1,n,k_x,k_y}(z)\right|^2+\left|\boldsymbol{\psi}_{4,n,k_x,k_y}(z)\right|^2\right\}\mathrm{d}z}{\int\left\{\sum\limits_{j=1}^{6}\left|\psi_{j,n,k_x,k_y}(z)\right|^2\right\}\mathrm{d}z},\\
P_{\mathrm{LH},n,k_x,k_y} &= \frac{100\int\left\{\left|\boldsymbol{\psi}_{21,n,k_x,k_y}(z)\right|^2+\left|\boldsymbol{\psi}_{3,n,k_x,k_y}(z)\right|^2\right\}\mathrm{d}z}{\int\left\{\sum\limits_{j=1}^{6}\left|\psi_{j,n,k_x,k_y}(z)\right|^2\right\}\mathrm{d}z},\\
P_{\mathrm{SO},n,k_x,k_y} &= \frac{100\int\left\{\left|\boldsymbol{\psi}_{5,n,k_x,k_y}(z)\right|^2+\left|\boldsymbol{\psi}_{6,n,k_x,k_y}(z)\right|^2\right\}\mathrm{d}z}{\int\left\{\sum\limits_{j=1}^{6}\left|\psi_{j,n,k_x,k_y}(z)\right|^2\right\}\mathrm{d}z}.
\end{aligned}
\tag{7}
$$

The character of subbands can be examined with $|\boldsymbol{K}_{//}|$ increasing. This is illustrated in Fig.2 for the first three hole subbands of a 10nm-thick silicon nanoplate. Under the zero stress condition, near the Γ point, the n=1 subband is purely HH-like in character. The n=2 subband, slightly mixed with an SO band, is mainly LH-like, while the n=3 subband, slightly mixed with an LH band, is mainly SO-like. As $\boldsymbol{K}_{//}$ increases along the [110] direction, it is clear that the nature of the bands is strongly mixed, and split-off holes contribute more than the light holes in the nature of each subband for $\boldsymbol{K}_{//} > 1.9 \times 10^9 \mathrm{m}^{-1}$. When $\boldsymbol{K}_{//} > 2.5 \times 10^9 \mathrm{m}^{-1}$, then P_{HH}:P_{LH}:P_{SO} $\cong$51:18:31 for an unstrained silicon nanoplate. It is rather surprising that as the ratio for each subband is almost invariable with stress increasing. However, at small values of $\boldsymbol{K}_{//}$, the strain introduces an extra coupling between the HH, LH, and SO subbands. The strong mixings between HH, LH and SO subbands can be seen in the low part of Fig.2. Under 2GPa of uniaxial stress along the [110] direction, near Γ point, the n=1 subband, slightly mixed with an HH band, is mainly LH-like. The n=2 subband, slightly mixed with both an LH band and an HH band, is SO-like. The n=3 subband, slightly mixed with both an LH band and an SO band, is mainly HH-like. Therefore, it is suggested that the nature of subbands is stress-dependent, that is, the stress determines the extent to which the band is mixed. In addition, a large anisotropy is also observed from Fig.2. We see that at large values of $|K_{//}|$ along the [100] direction, the ratio, P_{HH}:P_{LH}:P_{SO}, is about 24:44:32, which is different from that along the [110] direction. This indicates that the contribution of LH band is significantly larger than that of the HH subband, implying that the hole transport and the electromechanical property along the [100] direction are governed largely by the properties of the LH band. In addition, it is also worth noticing that the spin–orbit coupling effect should be considered in hole study, especially in a highly strained silicon nanoplate, for the contribution of SO band is significantly large in the LH band.

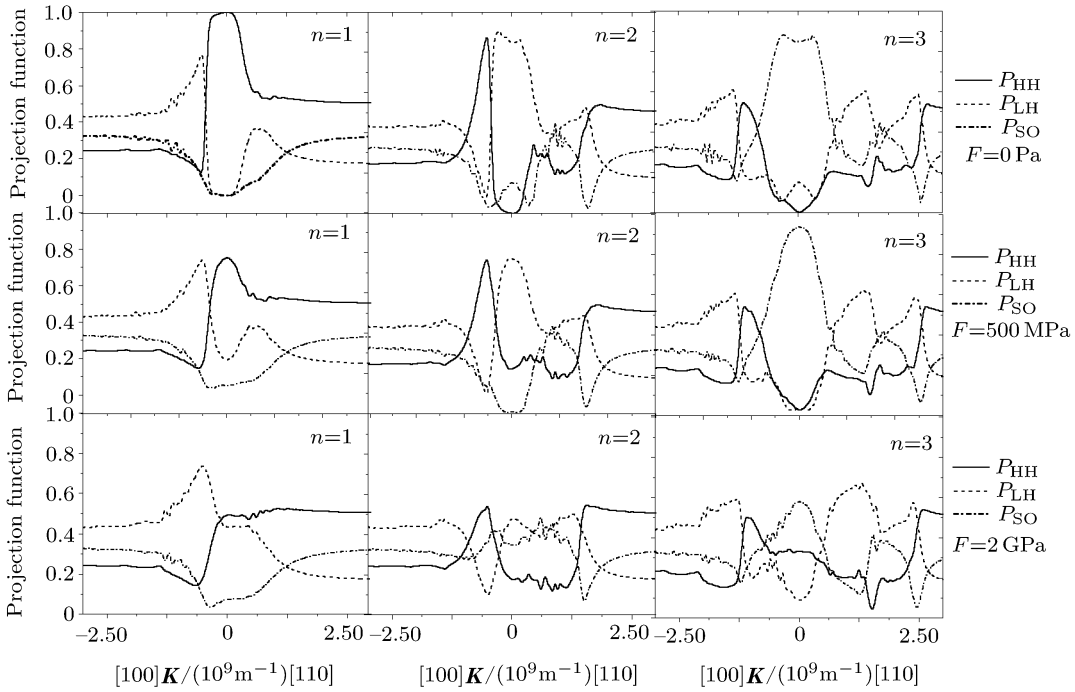


Fig.2. Natures of band (percentage) vs $\boldsymbol{K}_{//}$, separately, along [100] and [110] directions for the first three subbands subject to different stresses: F=0 Pa for top panels, F=500 MPa for middle panels, and F=2GPa for bottom panels.

3.2. Piezoresistive coefficients

The electromechanical property or the piezoresistance effect is defined as the change in electrical resistivity of solid when it is subjected to stress fields. It is well known that piezoresistance effect can be characterized by the piezoresistive coefficient. As discussed above, it can be defined in terms of the change in carrier concentration and the change in effective mass of hole as follows:

$$\pi = -\frac{1}{\boldsymbol{X}} \frac{\sum\limits_{i=1}^{n} \left(\frac{\Delta p_i}{p} \frac{1}{m_i} + \frac{p_i}{p} \Delta \left(\frac{1}{m_i} \right) \right)}{\sum\limits_{i=1}^{n} \frac{p_i}{p} \frac{1}{m_i}}. \qquad (8)$$

where p_i is the hole number per unit area in each subband, $p = \sum p_i$ is the total number of holes per unit area obtained from expression (5). $\Delta(1/m_i)$ is the mass shift upon the application of stress, and m_i is the effective mass of hole, which is defined as the inverse of the curvature of the valence subbands as shown below:

$$m_i = -\hbar^2 \left[\frac{\partial^2 \boldsymbol{E}}{\partial \boldsymbol{K}_{//}^2} \right]^{-1}. \qquad (9)$$

Once the energy spectra in silicon nanoplate are calculated for the cases with and without uniaxial stresses, separately, the change in effective mass, $\Delta(1/m_i)$, can be obtained from the above expression.

Figure 3 shows the variations in hole occupation at 300K as a function of thickness in the cases with and without stresses. It is observed that at a stress of 0.1GP a slight change in hole occupation takes place. However, the hole occupation dramatically changes with the thickness of the silicon nanoplate decreasing. As the thickness decreases from 14 to 3nm, the hole occupation of the n=1 subband increases monotonically, while those of the n=2 subband and the n=3 subband decrease monotonically. This change is attributed primarily to the enhancement of the quantum confinement of holes, which results in increasing the separation of the subbands, leading to a carrier repopulation in favour of the HH subband.

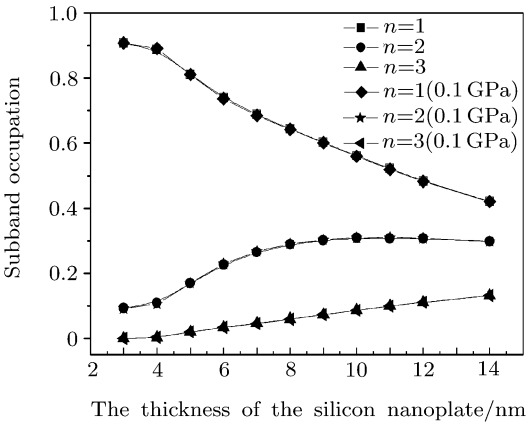


Fig.3. The variations in subband occupation with thickness in the cases with and without stresses.

To calculate the piezoresistive coefficient, it is necessary to obtain the variation in valence-band effective mass. Considering the concentration of the carriers in the n=3 subband is not negligible, the change in effective mass has been calculated for the first three subbands. In Fig.4, the variations in effective mass are depicted as a function of the thickness in the cases with and without stresses. It is important to note that the bulk HH mass, the LH mass and the SO mass in the [110] direction are 0.62, 0.15, and $0.24m_0$, respectively. The panels clearly show that the effective masses of a silicon nanoplate below 20nm are not governed by bulk properties. However, it is observed that the effective masses approach the bulk value as the thickness increases. The quantization effective masses of the n=1 hole band are almost independent of the thickness for unstrained silicon nanoplate below 20nm. This is expected because this subband is purely HH-like at the band minimum as shown in Fig.2. However, the results are quite different from those for n=2 or n=3 subband due to band mixing.

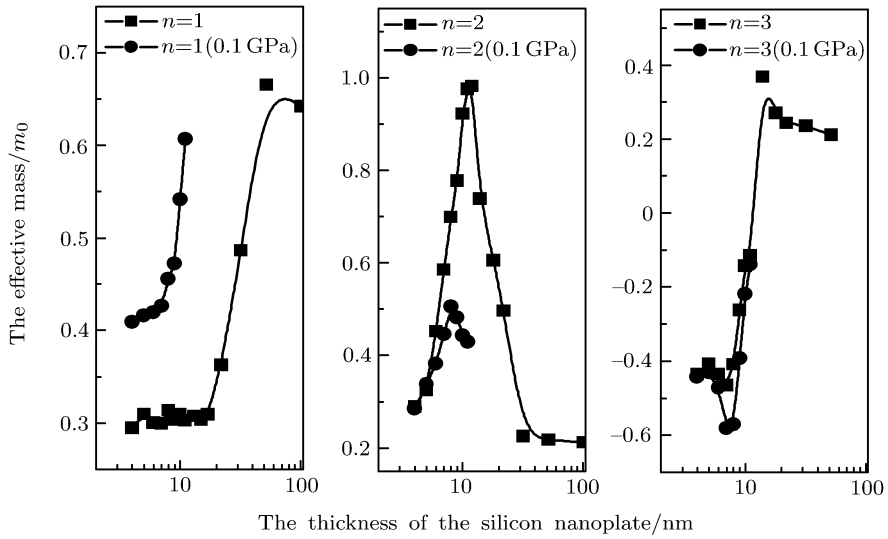


Fig.4. The thickness dependence of valence-band effective mass in the cases with and without stresses.

Based on the hole concentration and effective mass in the cases with and without stresses, the dependences of the piezoresistive coefficient on thickness or temperature are quantitatively investigated in the following. The variation in piezoresistive coefficient with the thickness is shown in Fig.5(a). The piezoresistive coefficient exhibits size dependence. It increases monotonically as the thickness of the silicon nanoplate decreases. The interaction of the piezoresistive effect with quantum confinement is the origin of this behaviour. As the thickness of the silicon nanoplate decreases, an increase in separation of the subbands results in an extra reduction in carrier mobility, which is mainly due to the changes in effective conduction mass and subband repopulation associated, hence, enhancing the piezoresistance effect. The piezoresistive coefficient increases about 4 times as the thickness decreases from the bulk to 3nm, exhibiting a promising application in mechanical sensors. However, this value is not as large as that given by Ref.[19] where only HH and LH couplings were taken into account, while our result is obtained by considering the band mixing among HH, LH, and SO bands. Note that the piezoresistive coefficient of the 10nm-thick silicon nanoplate obtained from our model is close to the calculated value.[12]

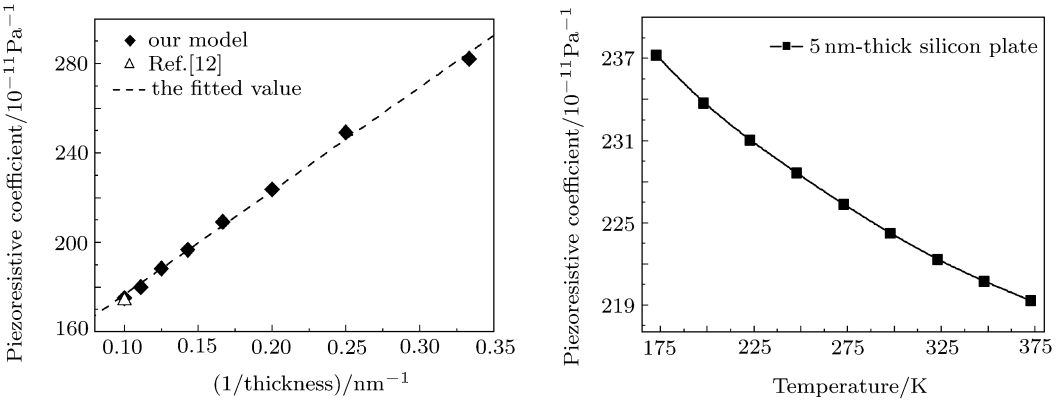


Fig.5. (a) Piezoresistive coefficients varying with thickness (a) and temperature (b) separately.

It is interesting to analyse the temperature dependence of the piezoresisitive coefficient for the silicon nanoplate. Typical p-type silicon mechanical sensors are designed to operate under temperatures ranging from 173 to 373 K. Figure 5(b) shows the calculated result of the piezoresistive coefficient as a function of temperature in this regime. The size-dependent piezoresistive coefficient is observed to decrease with temperature increasing. This is mainly due to the redistribution of the carriers between the HH, LH and SO subbands. However, the piezoresistive coefficient decreases only by almost 7.5% for a change in temperature from 173 to 373 K. At room temperature, the piezoresistive coefficient of a 5nm-thick silicon nanoplate reaches as high as 224.2×10^{-11} Pa^{-1} compared with a bulk value of 71×10^{-11} Pa^{-1} for the case with an impurity concentration of 1×10^{17}/cm^3.

4. Conclusions

The Schrödinger equation and the Poisson equation are solved in an iterative process to obtain the subband structure of a p-type single-crystal silicon nanoplate. It shows that hole quantization effect and the hole band mixing as well as the spin–orbit coupling effect should be taken into account in order to describe appropriately the subband structure and the electromechanical property. Due to the band mixing and the spin–orbit coupling, all subband dispersions are strongly anisotropic, far from parabolic, and at small values of $\boldsymbol{K}_{//}$, a stress can introduce an extra coupling between the HH, LH, and SO subbands, which has an influence on the nature of subband. Our result also indicates that the piezoresistive coefficient is size-dependent due to the interaction of the piezoresistive effect with hole quantization effect. In particular, at room temperature, the piezoresistive coefficient of a 5nm-thick silicon nanoplate reaches as high as 224.2×10^{-11}Pa^{-1} compared with a bulk value of 71×10^{-11}Pa^{-1} for the case with an impurity concentration of 1×10^{17}/cm^3. Furthermore, the size-dependent piezoresistive coefficient is observed to slightly decrease with temperature increasing.

References

[1] Smith C S 1954 *Phys. Rev.* **94** 42

[2] Tufte O N and Stelzer E L 1963 *J. Appl. Phys.* **34** 313

[3] Guo S W, Tan S S and Wang W Y 1988 *Acta Phys. Sin.* **37** 1794 (in Chinese)

[4] Namazu T, Isono Y and Tanaka T 2000 *J. Microelectromech. Syst.* **9** 450

[5] Duval F F C, Wilson S A, Ensell G, Evanno N M P, Gain M G and Whatmore R W 2007 *Sensors and Actuators* A **133** 35

[6] Kleimann P, Semmache B, Berre M L and Barbier D 1998 *Phys. Rev.* B **57** 8966

[7] Toriyama T and Sugiyama S 2002 *J. Microelectromech. Syst.* **11** 598

[8] Matsuda K 2004 *J. Comput. Electron.* **3** 273

[9] Guillaume T and Mouis M 2006 *Solid-State Electronics* **50** 701

[10] Kozlovskiy S I, Nedostup V V, and Boiko I I 2007 *Sensors and Actuators* A **133** 72

[11] Rosa A L, Scolfaro L M R, Enderlein R, Sipahi G M and Leite J R 1998 *Phys. Rev.* B **58** 15675

[12] Ivanov T, Gotszalk T, Sulzbach T and Rangelow I W 2003 *Ultramicroscopy* **97** 377

[13] Wu Z M, Lei Q S, Geng X H, Zhao Ying, Sun J and Xi J P 2006 *Chin. Phys.* **15** 320

[14] Wang J L and W E X 2007 *Chin. Phys.* **16** 848

[15] He R R and Yang P D2006 *Nature Nanotechnology* **1** 42

[16] Xing Y J, Yu D P, Xi Z H and Xue Z Q 2002 *Chin. Phys.* **11** 1047

[17] Harley J A and Kenny T W 1999 *Appl. Phys. Lett.* **75** 289

[18] Toriyama T, Tanimoto Y and Sugiyama S 2002 *J. Microelectromech. Syst.* **11** 605

[19] Pramanik C, Banerjee S, Saha H and Sarkar C K 2006 *Nanotechnology* **17** 3209

[20] Lee J and Vassell M O 1988 *Phys. Rev.* B **37** 8855

[21] Chao C Y and Chuang S L 1992 *Phys. Rev.* B **46** 4110

[22] Sun Y, Thompson S E and Nishida T 2007 *J. Appl. Phys.* **101** 104503

[23] Sun L, Yang W W, Xiang C L, Yu Z P and Tian L L 2005 *Chin. J. Semiconductors* **26** 2344

[24] Rodríguez S, López-Villanueva J A, Melchor L and Carceller J E 1999 *J. Appl. Phys.* **86** 438